AGU PUBLICATIONS

Geophysical Research Letters

RESEARCH LETTER
10.1002/2014GL062196

Key Points:
- TGFs are produced near 12 km between the charge layers of a thunderstorm
- TGFs contain approximately 10^{18} runaway electrons
- The electric current in the TGF generation process can be very strong

Correspondence to:
S. A. Cummer,
cummer@ee.duke.edu

Citation:
Cummer, S. A., M. S. Briggs, J. R. Dwyer, S. Xiong, V. Connaughton, G. J. Fishman, G. Lu, F. Lyu, and R. Solanki (2014), The source altitude, electric current, and intrinsic brightness of terrestrial gamma ray flashes, *Geophys. Res. Lett.*, *41*, doi:10.1002/2014GL062196.

Received 13 OCT 2014
Accepted 3 NOV 2014
Accepted article online 6 NOV 2014

The source altitude, electric current, and intrinsic brightness of terrestrial gamma ray flashes

Steven A. Cummer[1], Michael S. Briggs[2], Joseph R. Dwyer[3], Shaolin Xiong[2], Valerie Connaughton[2], Gerald J. Fishman[4], Gaopeng Lu[5,6], Fanchao Lyu[1], and Rahulkumar Solanki[1]

[1]Electrical and Computer Engineering Department, Duke University, Durham, North Carolina, USA, [2]CSPAR, University of Alabama in Huntsville, Huntsville, Alabama, USA, [3]Department of Physics, University of New Hampshire, Durham, New Hampshire, USA, [4]Earth Systems Science Center, University of Alabama in Huntsville, Huntsville, Alabama, USA, [5]Key Laboratory of Middle Atmosphere and Global Environment Observation, Institute of Atmospheric Physics, Chinese Academy of Sciences, Beijing, China, [6]Collaborative Innovation Center on Forecast and Evaluation of Meteorological Disasters, Nanjing University of Information Science and Technology, Nanjing, China

Abstract Many details of how thunderstorms generate terrestrial gamma ray flashes (TGFs) and other forms of high-energy radiation remain uncertain, including the basic question of where they are produced. We exploit the association of distinct low-frequency radio emissions with generation of terrestrial gamma ray flashes (TGFs) to directly measure for the first time the TGF source altitude. Analysis of two events reveals source altitudes of 11.8 ± 0.4 km and 11.9 ± 0.9 km. This places the source region in the interior of the thunderstorm between the two main charge layers and implies an intrinsic TGF brightness of approximately 10^{18} runaway electrons. The electric current in this nontraditional lightning process is found to be strong enough to drive nonlinear effects in the ionosphere, and in one case is comparable to the highest peak current lightning processes on the planet.

1. Introduction

One of the most surprising modern discoveries in atmospheric electricity is that thunderstorms generate terrestrial gamma ray flashes (TGFs) [*Fishman et al.*, 1994] and associated high-energy electrons [*Dwyer et al.*, 2008], positrons [*Briggs et al.*, 2011], and perhaps neutrons [*Chilingarian et al.*, 2010]. The relativistic runaway electron avalanche process [*Gurevich et al.*, 1992; *Dwyer et al.*, 2012] is widely agreed to be the root cause, but fundamental questions remain open. There are several distinct theories about how the relativistic runaway electron avalanche (RREA) process is initiated and developed [*Dwyer*, 2008; *Celestin et al.*, 2012]. Moreover, observational limitations mean that estimates of how often TGFs occur range from rarely [*Smith et al.*, 2011] to commonly [*Østgaard et al.*, 2012].

A critical but unknown parameter linked to basic TGF properties such as intrinsic brightness and occurrence rate, and which may prove valuable for distinguishing the underlying physics, is the TGF source altitude. This was originally thought to be at mesospheric altitudes [*Taranenko and Roussel-Dupré*, 1996], but it was later shown that only lower source altitudes were possible due to modest charge moment changes in the associated lightning [*Cummer et al.*, 2005]. TGF spectral analysis has more tightly constrained the source altitude to below 20 km [*Dwyer and Smith*, 2005], which has been confirmed by additional measurements and analysis [*Carlson et al.*, 2007; *Gjesteland et al.*, 2010; *Marisaldi et al.*, 2014].

Radio measurements have provided some additional information. *Stanley et al.* [2006] were the first to show that TGFs are produced during positive polarity in-cloud lightning processes, and not by cloud-to-ground strokes, by analyzing radio emissions near the time of the TGF. Further analysis (similar to what we perform here) for two TGFs placed radio sources that occurred within several milliseconds of the TGFs at 11.5 and 13.6 km altitude. However, these measurements did not provide the source altitude of TGFs because timing uncertainty prevented connection of the TGF to specific radio emissions, and thus, it was not clear where and when the TGFs were produced. *Shao et al.* [2010] and *Lu et al.* [2010] showed through several more examples that TGFs were produced at some time during upward intracloud leader propagation between roughly 10 and 15 km, but again the timing uncertainty prevented any direct insight into the altitude where the TGF actually originated.

Here we exploit the association of the TGF-generating process with simultaneous and distinct low-frequency radio emissions [*Cummer et al.*, 2011; *Connaughton et al.*, 2013], and the reflected multipath propagation of such a signal with an elevated source, to directly measure the source altitude of two TGFs. The resulting altitudes are close to 12 km and imply about 5 times higher instrinsic brightness ($\sim 10^{18}$ runaway electrons) than most previous simulations have assumed and place the source region in the interior of the thunderstorm between the two main charge layers. The source current moment for one of these TGFs reaches above 500 kA km, showing that this nontraditional in-cloud lightning process is not only strong enough to drive nonlinear effects in the ionosphere [*Barrington-Leigh and Inan*, 1999] but is among the highest peak current lightning processes on the planet.

2. Instruments and Data

The TGF photons in the events analyzed here were observed by the Gamma-ray Burst Monitor (GBM) instrument on the Fermi satellite [*Briggs et al.*, 2010] and were identified in the GBM ground-search procedure [*Briggs et al.*, 2013]. The simultaneous radio emissions were recorded with a two-axis magnetic field sensor with a 1–300 kHz bandwidth deployed at the Florida Institute of Technology and located at 28.062°N latitude and −80.624°E longitude. The sensor has a flat frequency response from 100 to 200 kHz and a frequency-proportional response from 1 to 100 kHz. Absolute amplitude calibration was obtained from both laboratory measurements and in-field cross calibration with other magnetic sensors. GPS timing for both the radio and photon measurements ensures absolute timing accuracy of several microseconds.

The TGFs analyzed here were carefully selected for this analysis based on several criteria. We require radio emissions with a clear ionospheric reflection of the TGF-associated pulse. This in turn requires a fast, low-noise, and high-amplitude source pulse, and also no other significant radio pulses overlapping the ground wave or ionospheric reflection. Events during local night are preferred, when the ionosphere is a better reflector, and also the distance from source to radio sensor needs to be less than 1000 km so that the direct and reflected waves are as temporally separated as possible. Independent geolocation of the lightning source region is also needed for the timing calculation to confirm that the radio pulse whose source altitude we are measuring is simultaneous with the TGF. The selection is significantly biased toward short TGFs with stronger and short-timescale radio emissions. There are a handful of events that meet these criteria in our database, and the two best were selected for analysis.

TGF1 was detected by GBM on 1 August 2011 at 02:57:17 UTC when Fermi was at 546.94 km altitude with a geographic footprint of 24.5157°N–84.9626°E (note that all locations and distances are based on the World Geodetic System 84 coordinate system). The National Lightning Detection Network (NLDN) reported this event as a +120 kA in-cloud pulse at 02:57:17.409 UTC and 22.5287°N–82.1604°E. The oceanic location resulted in a relatively large (1.2 km) reported 50% geolocation error ellipse semimajor axis. This is 632 km from the FT sensor and 361 km from the Fermi footprint at the time of the TGF.

TGF2 was detected by GBM on 25 September 2013 at 05:25:13 UTC when Fermi was at 537.40 km altitude with a geographic footprint of 23.7092°N–84.3753°E. An NLDN geolocation with approximately 5 km accuracy is 28.34°N–86.24°E (normal processing failed because most nearby sensors were saturated by the event). Time difference of arrival analysis from our five LF stations yield a location of 28.34°N–86.29°E. The Earth Networks Total Lightning Network reported a location for this event of 28.342°N–86.292°E. We assume this last location in the analysis and conservatively estimate the location uncertainty at 2–3 km. This is 557 km from the FT sensor and 548 km from the Fermi footprint at the time of the TGF.

Figure 1a shows a map of the relevant locations for these two events. Assuming a 12.0 km source altitude for the TGF photons, Figures 1b and 1c show the recorded LF radio signals and TGF photon arrival times, referenced back to the source by subtracting the speed of light propagation time for each. Only the gamma rays detected with the higher-energy (>200 keV) bismuth germanate (BGO) detectors [*Briggs et al.*, 2010] are shown so that delayed, lower energy Compton-scattered photons are deemphasized, and the photon arrival time reflects the actual photon generation time.

It is critical to show that the simultaneity of the TGF photon pulse and the LF radio pulse holds in these two cases in order to argue that they occur at the same time and place [*Cummer et al.*, 2011; *Connaughton et al.*, 2013; *Dwyer and Cummer*, 2013]. Restricting the timing analysis to BGO-detected photons, which is necessary given the short duration of these TGFs, does not leave enough photons (11 and 14, respectively)

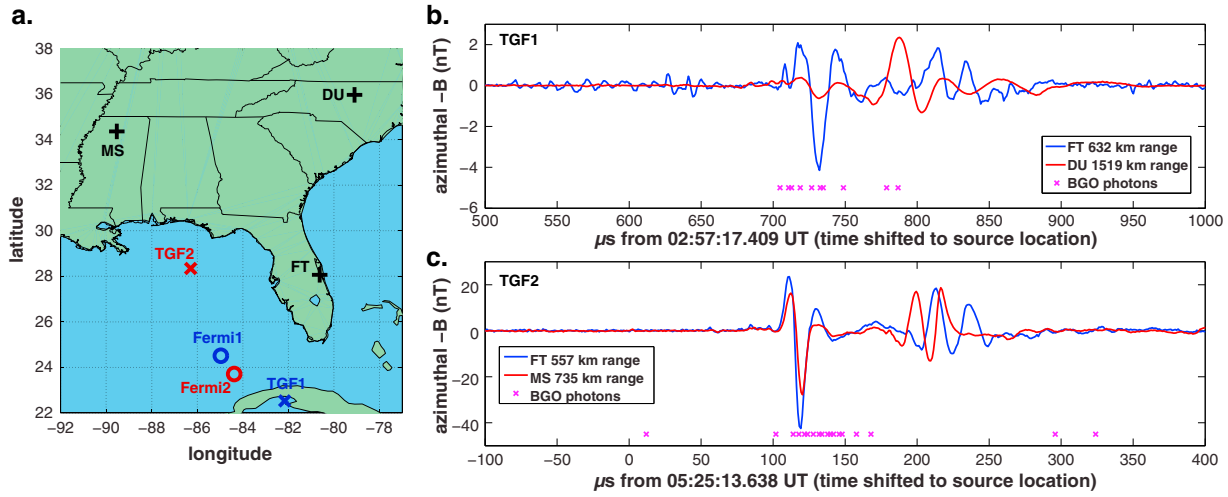

Figure 1. Overview and timing of the 2 TGFs. (a) Map showing the locations of the TGF source regions, Fermi satellite footprints, and LF sensors. (b) Recorded LF signals and GBM gamma ray arrival times for TGF1, back propagated to the source location. (c) Recorded LF signals and GBM gamma ray arrival times for TGF2, back propagated to the source location.

to bin into statistically meaningful time profiles as done by *Cummer et al.* [2011]. We can thus best evaluate simultaneity by examining the start times and durations of the photon and radio pulses in Figures 1b and 1c.

In both cases, the first photon that is clearly part of the TGF occurs within 10 μs of the start of the LF ground wave pulse. This level of time discrepancy is consistent with the possible horizontal source location uncertainty of several kilometers, and thus, the signal onsets are effectively simultaneous. The durations of TGF1 and TGF2 are 44 and 34 μs, respectively, although there is notable energy dispersion in both cases, and it is possible that the true source durations were even shorter. The durations of the LF radio pulses (which appear as tripolar pulses due to the frequency response of the sensors) are 46 and 33 μs, respectively.

This confirms the simultaneity of the photon and radio emissions in these two events, which in turn strongly suggests that the radio emissions are at least partly and perhaps entirely from the TGF-generating process [*Cummer et al.*, 2011; *Dwyer*, 2012; *Connaughton et al.*, 2013; *Dwyer and Cummer*, 2013] and that these two processes are coincident in time and space. Throughout the remaining analysis, we thus assume that the altitude of radio emission is the altitude of the TGF generation.

3. TGF Source Altitude Analysis

The LF radio emissions in Figures 1b and 1c show that the first ionospheric reflected pulse shifts closer to the ground wave as propagation distance increases and that the reflected pulses from both TGFs at the FT sensor are composed of two distinct peaks. This is the signature of an aboveground source, and the relative peak timing can be used to accurately estimate that source altitude [*Smith et al.*, 2004].

We use a simple ground wave-only propagation model [*Dwyer and Cummer*, 2013] to estimate the source current moment waveform for each event. A simple Gaussian source reproduces more than 95% of the energy in the measured ground wave signal in both events (full width at half maxima of 16.8 and 11.2 μs). The extracted source current moment waveforms are shown in Figure 2a. The total charge moment changes for these are 2.1 and 6.5 C km, respectively.

Our extraction of the source altitude is based on a detailed comparison of measured and simulated magnetic field waveforms. To make as accurate an estimate as possible given the complicated frequency-dependent reflectivity of a realistic ionosphere, we use the extracted source current moment waveforms as the source term in a numerical simulation of very low frequency and low-frequency electromagnetic wave propagation in the Earth-ionosphere waveguide [*Hu and Cummer*, 2006]. The height of the ionosphere plays a modest role in the relative timing of the two ionospherically reflected pulses and thus also must be estimated.

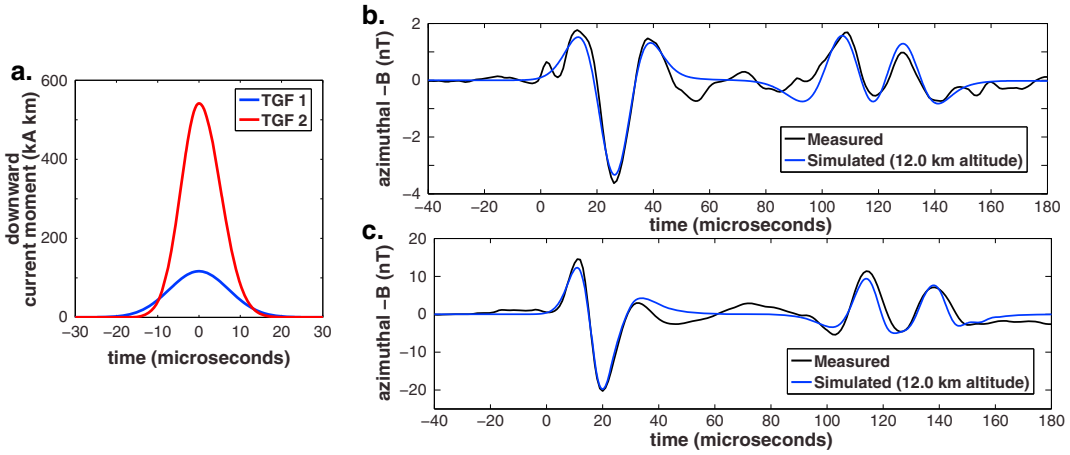

Figure 2. TGF waveforms and source current. (a) Gaussian current moment waveforms that accurately reproduce the observed ground wave radio pulses. (b) Agreement between the measured and simulated LF signal for TGF1 assuming a source altitude of 12.0 km, showing that the two later pulses are the expected ionospheric reflections. (c) Agreement between the measured and simulated LF signal for TGF2 assuming a source altitude of 12.0 km, again showing that the two later pulses are the expected ionospheric reflections.

We assume a two-parameter exponential electron density profile [*Cummer et al.*, 1998], and for each event we vary the effective height parameter (h') in 1 km steps to match the relative timing of the ground and sky waves for the known propagation distance. This results in $h' = 90$ and 92 km for TGF1 and TGF2, respectively, and simulations with these electron density profiles are used in the analysis. The measured and simulated fields for TGF1 and TGF2 are shown in Figures 2b and 2c, respectively, for an assumed source altitude of 12.0 km.

From simple geometric calculations using the distances involved, a shift in h' of 1 km shifts the arrival time of both reflected pulses by approximately 2 μs, and such a shift clearly moves the midpoint of the reflected pulses to visible disagreement with the data. Also, a 1 km change in h' changes the time difference between the two reflected pulses by 240 ns, which is equivalent to a source altitude change of 120 m. This is much smaller than the uncertainty due to measurement noise (see section 4), so any uncertainties in h' tuning do not affect the final measurements. The good agreement confirms that the observed pair of pulses 100–140 μs after the ground wave are the ionospheric reflections of the sources shown in Figure 2a.

Figures 3a and 3b show, for TGF1 and TGF2, respectively, the simulated ionospherically reflected pulse pair waveform as a function of source altitude from 10.0 to 15.0 km, overlaid on the measurements. In both cases, as the source altitude increases, the pulse separation increases, and the relative amplitude of individual peaks also changes from mutual interference. These differences are sufficient to constrain the source altitude of the TGF-associated pulse. Visual inspection suggests that a source between 11 and 12 km appears to be the best fit in each case.

To estimate the source altitude more precisely, we calculate the normalized cross-correlation peak of the measured and simulated waveforms (normalized by the product of the 2 norm of each so that perfect agreement is unity) as a function of source altitude with 0.5 km resolution and then interpolate to 0.1 km resolution. This gives the same curve that would be obtained with 0.1 km resolution simulations but at lower computational cost. These curves are shown in 3c, and for each the maximum normalized cross correlation gives the best fit source altitude. This is 11.9 km for TGF1, and 11.8 km for TGF2. That these two events, 2 years apart, resulted in nearly identical source altitudes is certainly at least in part coincidence, as the altitudes of these two storms were almost identical (which is discussed in section 5). Nevertheless, it suggests the possibility that there may be a "sweet spot" for TGF generation, above which the strong electric fields needed for TGF production do not occur, and below which there is too much atmospheric attenuation of the gamma ray beam to be detected on orbit.

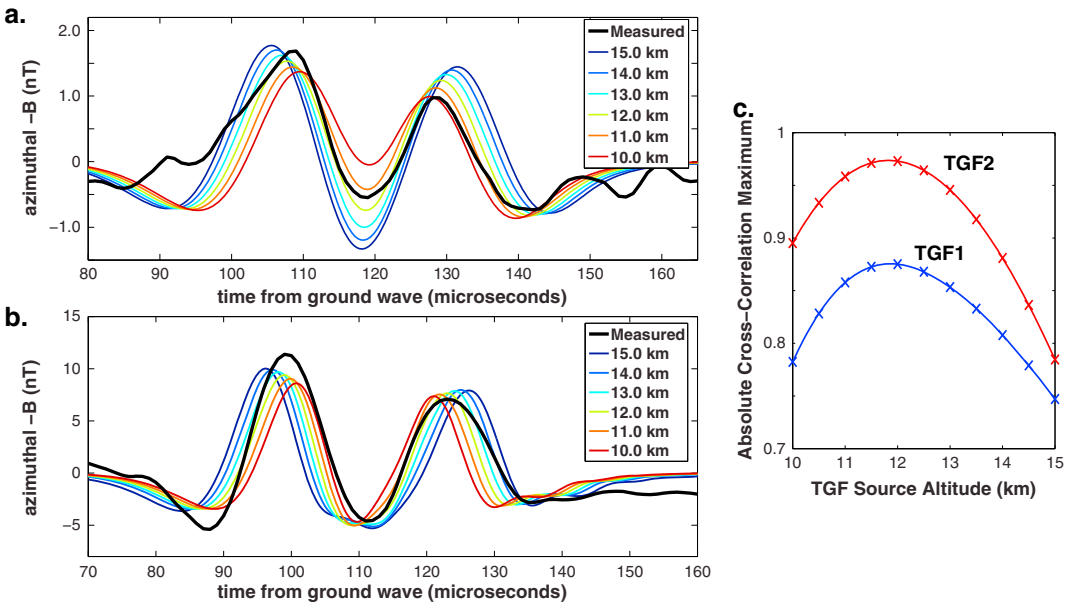

Figure 3. TGF source parameter extraction. (a) Comparison between the measured and simulated ionospherically reflected signal for TGF1 as a function of source altitude, showing that the pulse separation can distinguish the source altitude. (b) The same comparison for TGF2, again showing that the reflected pulse separation distinguishes the source altitude. (c) The maximum cross correlation of the measured and simulated ionospherically reflected signal versus source altitude, for TGF1 and TGF2. The peaks are at 11.9 km for TGF1 and 11.8 km for TGF2.

4. Altitude Measurement Uncertainty

The uncertainty in these altitude measurements plays a critical role in their interpretation. We estimate the measurement uncertainty through the following Monte Carlo procedure. We create thousands of synthetic "data" waveforms by adding noise realizations to a noiseless finite difference time domain-simulated waveform produced using a known source altitude (12.5 km in this case). The statistical parameters of the power spectrum of this noise are chosen to be consistent with the observed noise computed by subtracting the best fit simulations from the two measured signals (as in Figures 3a and 3b). The noise amplitude is varied in these realizations so that the synthetic data waveforms span a wide range of signal-to-noise ratio (SNR) to fully quantify the relationship between noise and altitude uncertainty. We then run our data analysis procedure on the synthetic data to find the source altitude that maximizes the cross correlation between the synthetic data and the variable altitude, noise-free simulations. This yields thousands of simulated source altitude errors (since the source altitude of the simulated data is known to be 12.5 km in each case).

The source altitude error is expected to depend on the SNR in the synthetic data and on the propagation distance. We perform the calculations that follow for a propagation distance of 600 km, which we have confirmed gives uncertainties effectively identical (within a few tens of meters) to those for the true propagation distances of 557 and 632 km. Significantly longer or shorter propagation distances would require additional analysis. We organize the simulated errors as a function of the maximum normalized cross correlation between the synthetic data and altitude-variable simulations. This cross-correlation maximum is directly related to SNR and, importantly, is known for the two real TGFs analyzed here (see Figure 3c). We bin the synthetic source altitude errors according to maximum cross correlation (and thus SNR) in bins that are 0.02 units wide, i.e., 0.98 to 1.0 and 0.97 to 0.99. Each bin then contains a statistical distribution of altitude errors for a narrow range of SNR. We then define the altitude uncertainty at a fixed SNR as the standard deviation of these altitude errors within a single SNR bin. Figure 4a shows six realizations of noisy synthetic data with a maximum cross correlation close to 0.97. Note the similarity of this synthetic data to the real data for TGF2 shown in Figure 2c, which has the same maximum cross correlation.

As an example, Figure 4b shows a histogram of the altitude error computed from more than 4400 synthetic data waveforms with maximum cross correlation of 0.97 $\pm$ 0.01. This is thus the expected altitude uncertainty distribution for this relatively high maximum cross correlation (and thus high SNR), and the standard

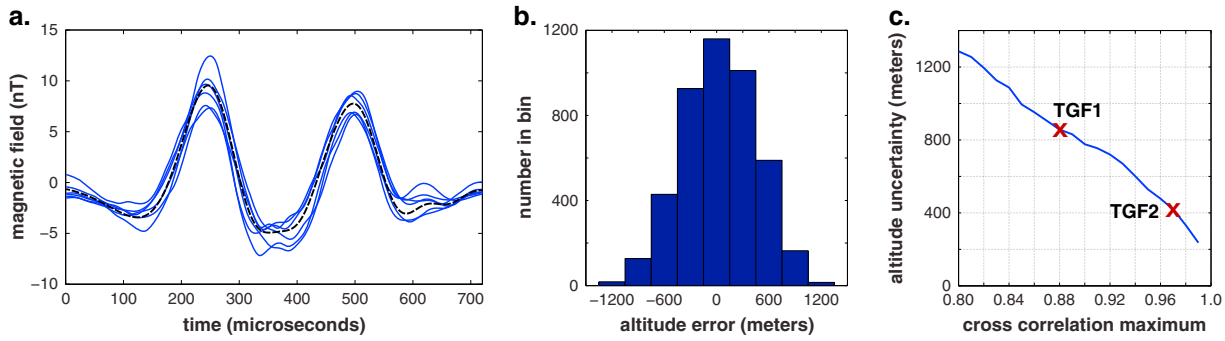

Figure 4. Source altitude measurement uncertainty for a propagation distance 600 km. (a) Six realizations of noisy synthetic data corresponding to a maximum cross correlation of 0.97, along with the original noiseless simulation in black. (b) Distribution of altitude error from 4400 realizations of noisy synthetic data with a maximum cross correlation of 0.97. The resulting standard deviation of 420 m is taken to be the source altitude measurement uncertainty for this level of noise, which corresponds to the measurements of TGF2. (c) Statistical source altitude measurement uncertainty as a function of cross-correlation maximum. The cross correlation maxima are 0.88 and 0.97 for TGF1 and TGF2, corresponding to altitude uncertainties of 860 m and 420 m, respectively.

deviation of this distribution is the altitude uncertainty for a maximum cross correlation of 0.97. The overall altitude uncertainty versus maximum cross-correlation maximum is shown in Figure 4c. As expected, the altitude uncertainty increases as the cross-correlation maximum decreases (and thus SNR decreases). The two TGFs analyzed here yielded cross correlation maxima of 0.88 and 0.97 (see Figure 3c), which are marked on Figure 4. We thus estimate the altitude measurement uncertainty to be $\pm$ 860 m for TGF1, and $\pm$ 420 m for TGF2.

5. Implications and Conclusions

Supporting measurements are consistent with previous observations and place the measured altitudes in the contexts of the originating storm. Radar scans of the two storms at the source locations reveal enhanced echo tops (18 dBz reflectivity) of approximately 13.5 km altitude in the vicinity of the TGF in both cases. Lower resolution satellite infrared images show cloud top temperatures at the TGF source regions of −60 to −65°C, indicating cloud tops of 13–13.5 km altitude according to local soundings. These storm altitudes are notably similar to those associated with a TGF over the United States [*Lu et al.*, 2010]. The very similar storm altitudes here are at least partly responsible for the nearly identical TGF source altitudes found for these two events.

The only lightning development stage that has been connected definitively to TGF generation is the initial upward propagating in-cloud leader, and TGFs occur during the leader ascent before reaching its maximum altitude [*Shao et al.*, 2010; *Lu et al.*, 2010]. Previous observations of upward leaders have placed the top leader altitude near 20 to 25 dBZ radar reflectivity [*Lu et al.*, 2011], which is 13–14 km altitude for the two storms here. Thus, the measured TGF source altitudes of 11.8 $\pm$ 0.4 km and 11.9 $\pm$ 0.9 km are, even with the uncertainties, in the region between the main charge centers where high electric fields are likely to be, and that the TGFs are generated while the upward propagating in-cloud leader is still ascending.

The source altitude constraints the intrinsic brightness of the TGF source. Modeling has shown that typical TGF on-orbit fluences require 2×10^{17} runaway electrons in the source region, assuming a 15 km source altitude [*Dwyer and Smith*, 2005]. Moving the source down to 12 km requires upward scaling of the energetic source electrons by a factor of about 5 [*Dwyer and Smith*, 2005; *Carlson et al.*, 2007; *Hansen et al.*, 2013], and typical TGFs thus require approximately 10^{18} runaway electrons in the source region (assuming a high field region of several hundred meters in length [*Dwyer and Cummer*, 2013]) and a comparable number of gamma rays. This shows that TGFs can occur at aircraft altitudes, and an intrinsically brighter source increases the possibility of significant radiation doses close to or in the source region [*Dwyer et al.*, 2010].

There are also some interesting implications of the TGF-associated current moment waveforms shown in Figure 2a. We reemphasize that the two events analyzed here were selected based on criteria that favor high peak current moment TGF-associated signals. Nevertheless, their timing confirms that they are produced during the TGF-generating electron acceleration process and thus are likely to have been generated by the RREA process, not a traditional lightning process. The relationship between the peak-extracted

current moment and NLDN-reported peak current for TGF1 (117 kA km and 120 kA) suggests that TGF2 (542 kA km) would have been reported by the NLDN as a >500 kA peak current event.

NLDN peak current estimates are computed from a distance-dependent scaling of the peak radiated field magnitude [*Cummins and Murphy*, 2009], and thus, a reported 500 kA NLDN peak current event generates the same peak radiated field regardless of whether it is an in-cloud event or a cloud-to-ground stroke. Thus, both of these TGFs, and particularly TGF2, radiate intensely enough to create elves, which are high-altitude (about 90 km) optical emissions generated by nonlinear processes excited by a strong lightning-generated electromagnetic pulse in the ionosphere [*Inan et al.*, 2010]. Moreover, the largest peak lightning currents measured by any method are on the order of several hundred kiloamperes, and this means that the TGF-generating process may be capable of generating some of the highest lightning-associated peak currents on the planet despite being a nontraditional lightning process.

Acknowledgments

The authors would like to acknowledge support from the National Science Foundation Dynamic and Physical Meteorology program through grant ATM-1047588 and the DARPA Nimbus program through grants HR0011-10-1-0059 and HR0011-10-1-0061. We thank Eric Cramer (Florida Institute of Technology) and Sumedhe Karunarathne (University of Mississippi) for leading the operation of the LF radio sensors used in this work. We thank Ken Cummins (Vaisala, Inc.) and Stan Heckman (Earth Networks, Inc.) for providing lightning geolocation data and analysis. We thank Lisa Gibby (Jacobs Technology), Matthew Stanbro (UA Huntsville) and Ger Fitzpatrick, Suzanne Foley, Sheila McBreen, and Dave Tierney (University College Dublin) for quickly finding TGFs in the GBM data. Fermi GBM data are publicly available through the Fermi Science Support Center. LF radio data for the two events analyzed here are available by request (cummer@ee.duke.edu). The numerical simulations used in the data interpretation are described in detail by *Hu and Cummer* [2006].

W.K. Peterson thanks two anonymous reviewers for their assistance in evaluating this paper.

References

Barrington-Leigh, C. P., and U. S. Inan (1999), Elves triggered by positive and negative lightning discharges, *Geophys. Res. Lett.*, *26*(6), 683–686.

Briggs, M. S., et al. (2010), First results on terrestrial gamma ray flashes from the Fermi Gamma-ray Burst Monitor, *J. Geophys. Res.*, *115*, A07323, doi:10.1029/2009JA015242.

Briggs, M. S., et al. (2011), Electron-positron beams from terrestrial lightning observed with Fermi GBM, *Geophys. Res. Lett.*, *38*, L02808, doi:10.1029/2010GL046259.

Briggs, M. S., et al. (2013), Terrestrial gamma-ray flashes in the Fermi era: Improved observations and analysis methods, *J. Geophys. Res. Space Physics*, *118*, 3805–3830, doi:10.1002/jgra.50205.

Carlson, B. E., N. G. Lehtinen, and U. S. Inan (2007), Constraints on terrestrial gamma ray flash production from satellite observation, *Geophys. Res. Lett.*, *34*, L08809, doi:10.1029/2006GL029229.

Celestin, S., W. Xu, and V. P. Pasko (2012), Terrestrial gamma ray flashes with energies up to 100 MeV produced by nonequilibrium acceleration of electrons in lightning, *J. Geophys. Res.*, *117*, A05315, doi:10.1029/2012JA017535.

Chilingarian, A., et al. (2010), Ground-based observations of thunderstorm-correlated fluxes of high-energy electrons, gamma rays, and neutrons, *Phys. Rev. D*, *82*(4), 043009, doi:10.1103/PhysRevD.82.043009.

Connaughton, V., et al. (2013), Radio signals from electron beams in terrestrial gamma ray flashes, *J. Geophys. Res. Space Physics*, *118*, 2313–2320, doi:10.1029/2012JA018288.

Cummer, S. A., U. S. Inan, and T. F. Bell (1998), Ionospheric D region remote sensing using VLF radio atmospherics, *Radio Sci.*, *33*(6), 1781–1792.

Cummer, S. A., Y. Zhai, W. Hu, D. M. Smith, L. I. Lopez, and M. A. Stanley (2005), Measurements and implications of the relationship between lightning and terrestrial gamma ray flashes, *Geophys. Res. Lett.*, *32*, L08811, doi:10.1029/2005GL022778.

Cummer, S. A., G. Lu, M. S. Briggs, V. Connaughton, S. Xiong, G. J. Fishman, and J. R. Dwyer (2011), The lightning-TGF relationship on microsecond timescales, *Geophys. Res. Lett.*, *38*, L14810, doi:10.1029/2011GL048099.

Cummins, K. L., and M. J. Murphy (2009), An overview of lightning locating systems: History, techniques, and data uses, with an in-depth look at the U.S. NLDN, *IEEE Trans. Electromagn. Compat.*, *51*(3), 499–518.

Dwyer, J. R. (2008), Source mechanisms of terrestrial gamma-ray flashes, *J. Geophys. Res.*, *113*, D10103, doi:10.1029/2007JD009248.

Dwyer, J. R. (2012), The relativistic feedback discharge model of terrestrial gamma ray flashes, *J. Geophys. Res.*, *117*, A02308, doi:10.1029/2011JA017160.

Dwyer, J. R., and S. A. Cummer (2013), Radio emissions from terrestrial gamma-ray flashes, *J. Geophys. Res. Space Physics*, *118*, 3769–3790, doi:10.1002/jgra.50188.

Dwyer, J. R., and D. M. Smith (2005), A comparison between Monte Carlo simulations of runaway breakdown and terrestrial gamma-ray flash observations, *Geophys. Res. Lett.*, *32*, L22804, doi:10.1029/2005GL023848.

Dwyer, J. R., B. W. Grefenstette, and D. M. Smith (2008), High-energy electron beams launched into space by thunderstorms, *Geophys. Res. Lett.*, *35*, L02815, doi:10.1029/2007GL032430.

Dwyer, J. R., D. M. Smith, M. A. Uman, Z. Saleh, B. Grefenstette, B. Hazelton, and H. K. Rassoul (2010), Estimation of the fluence of high-energy electron bursts produced by thunderclouds and the resulting radiation doses received in aircraft, *J. Geophys. Res.*, *115*, D09206, doi:10.1029/2009JD012039.

Dwyer, J. R., D. M. Smith, and S. A. Cummer (2012), High-energy atmospheric physics: Terrestrial gamma-ray flashes and related phenomena, *Space Sci. Rev.*, *173*, 133–196, doi:10.1007/s11214-012-9894-0.

Fishman, G. J., et al. (1994), Discovery of intense gamma-ray flashes of atmospheric origin, *Science*, *264*(5163), 1313–1316.

Gjesteland, T., N. Østgaard, P. H. Connell, J. Stadsnes, and G. J. Fishman (2010), Effects of dead time losses on terrestrial gamma ray flash measurements with the Burst and Transient Source Experiment, *J. Geophys. Res.*, *115*, A00E21, doi:10.1029/2009JA014578.

Gurevich, A. V., G. M. Milikh, and R. Roussel-Dupre (1992), Runaway electron mechanism of air breakdown and preconditioning during a thunderstorm, *Phys. Lett. A*, *165*, 463–468.

Hansen, R. S., N. ØStgaard, T. Gjesteland, and B. Carlson (2013), How simulated fluence of photons from terrestrial gamma ray flashes at aircraft and balloon altitudes depends on initial parameters, *J. Geophys. Res. Space Physics*, *118*, 2333–2339, doi:10.1002/jgra.50143.

Hu, W., and S. A. Cummer (2006), An FDTD model for low and high altitude lightning-generated EM fields, *IEEE Trans. Antennas Propag.*, *54*(5), 1513–1522.

Inan, U. S., S. A. Cummer, and R. A. Marshall (2010), A survey of ELF and VLF research on lightning-ionosphere interactions and causative discharges, *J. Geophys. Res.*, *115*, A00E36, doi:10.1029/2009JA014775.

Lu, G., et al. (2010), Lightning mapping observation of a terrestrial gamma-ray flash, *Geophys. Res. Lett.*, *37*, L11806, doi:10.1029/2009GL038880.

Lu, G., et al. (2011), Lightning development associated with two negative gigantic jets, *Geophys. Res. Lett.*, *38*, L12801, doi:10.1029/2011GL047662.

Marisaldi, M., et al. (2014), Properties of terrestrial gamma ray flashes detected by AGILE MCAL below 30 MeV, *J. Geophys. Res. Space Physics*, *119*, 1337–1355, doi:10.1002/2013JA019301.

Østgaard, N., T. Gjesteland, R. S. Hansen, A. B. Collier, and B. Carlson (2012), The true fluence distribution of terrestrial gamma flashes at satellite altitude, *J. Geophys. Res.*, *117*, A03327, doi:10.1029/2011JA017365.

Shao, X., T. Hamlin, and D. M. Smith (2010), A closer examination of terrestrial gamma-ray flash-related lightning processes, *J. Geophys. Res.*, *115*, A00E30, doi:10.1029/2009JA014835.

Smith, D. A., M. J. Heavner, A. R. Jacobson, X. M. Shao, R. S. Massey, R. J. Sheldon, and K. C. Wiens (2004), A method for determining intracloud lightning and ionospheric heights from VLF/LF electric field records, *Radio Sci.*, *39*, RS1010, doi:10.1029/2002RS002790.

Smith, D. M., et al. (2011), The rarity of terrestrial gamma-ray flashes, *Geophys. Res. Lett.*, *38*, L08807, doi:10.1029/2011GL046875.

Stanley, M. A., X.-M. Shao, D. M. Smith, L. I. Lopez, M. B. Pongratz, J. D. Harlin, M. Stock, and A. Regan (2006), A link between terrestrial gamma-ray flashes and intracloud lightning discharges, *Geophys. Res. Lett.*, *33*, L06803, doi:10.1029/2005GL025537.

Taranenko, Y., and R. Roussel-Dupré (1996), High altitude discharges and gamma-ray flashes: A manifestation of runaway air breakdown, *Geophys. Res. Lett.*, *23*, 571–574, doi:10.1029/95GL03502.